Micro-optical grayscale excitation lenses for atom and ion trapping

D.A. Scrymgeour*, S.A. Kemme, R.R. Boye, A.R. Ellis, T.R. Carter, S. Samora, J.D. Hunker
Sandia National Laboratories, 1515 Eubank Blvd SE, Albuquerque, NM 87123

ABSTRACT

Designing and integrating micro-optical components into atom and ion traps are enabling steps toward miniaturizing trap dimensions in quantum computation applications. The micro-optic must have a high numerical aperture for precise illumination of the ion and should not introduce scatter. Due to the extreme optical efficiency requirements in trapped ion and atom-based quantum information processing, even slight losses from integrated micro-optics are detrimental.

We have designed and fabricated aspheric micro-lenses through grayscale transfer into a fused silica in an effort to realize increased transmissive efficiency and decreased scatter compared to an equivalent diffractive optical element. The fabricated grayscale lens profile matched the desired lens profile well, and the measured and predicted optical performances were in good agreement. The pattern was transferred via coupled plasma reactive-ion etching smoothly into the fused silica with a RMS roughness ~ 35 nm. The micro-lens had a diameter of 88 um and 14.2 um sag, with an as-designed focal length of 149 um and spot diameter of 2.6 um. The maximum measured efficiency was ~80% (86% of theoretical, possibly due to rms roughness). This realized efficiency is superior to the equivalent diffractive lens efficiency, designed to the same use parameters. The grayscale approach demonstrated an increase in collection efficiency, at the desired optical focal length, providing the potential for further refinement.

Keywords: Grayscale optics, micro-optics, ion trapping, quantum computation

1. INTRODUCTION

Trapped, laser-cooled ion qubits is a very promising technology that has already demonstrated many of the requirements for quantum information processing, a step on the way toward implementation of quantum computations.[1-3] In this scheme, ions trapped above a surface by RF potential fields are laser cooled to the ground state. Transitions are induced by optical excitation at resonant wavelengths and sensed by collecting ion fluorescence. To develop fault-tolerant quantum computing, readout fidelities >99.9% are required that necessitate the collection of the maximum amount of ion fluorescence.[4] To accomplish this, high numerical aperture micro-optics can be closely integrated with the ion traps. This would both decrease the computation time (more collected photons in a given time) and secondarily, accomplish a miniaturization of system, a critical component of future quantum computation.[5] Miniaturizing both the ion trap as well as the associated optics is a key component toward this milestone.[6]

Trapped ions which are stored in surface electrode traps provide a promising platform for quantum computing.[7,8] One particular computational function, qubit readout, is achieved by driving a resonant transition which involves only one qubit state, and measuring the presence or absence of fluorescence from the ion. In our case, a trapped Ca^+ ion is excited by 397 nm light from the ground $S_{1/2}$ to an excited $P_{1/2}$ level to detect its quantum state. Since the trapped ions are inherently sensitive to the excitation wavelength, unintentionally scattered 397nm light is a particular concern for implementing dense arrays of trapped ions. This imposes very low scattering levels to avoid decoherence of neighboring trapped ions.

Recently, an integrated array of diffractive lenses in dielectric coupled to an optical fiber array was realized to collect light emitted from a trapped ion at a distance of only 165 μm which greatly increased the numerical aperture of the collecting optical system.[9] While diffractive elements offer an elegant solution for high efficiency light collection, illumination/excitation of the ion with diffractive optics offers different challenges. In the excitation case efficiency isn't the primary concern; instead, the concern is maximum delivery of excitation light only to the desired ion. There is concern that light diffracted into other modes will negatively affect performance of more densely packed trapped ions. To address the issue of diffractively scattered light, this work discusses the development of an equivalent refractive lens created by grayscale processing. Such a refractive lens would not have diffractive scattering issues and could theoretically be the most efficient way to focus light on a trapped ion while maintaining the advantages of micro-optics integration.

*dscrymg@sandia.gov

Our refractive micro-lenses were created by grayscale lithography. In this technique, a spatially variable optical density mask is used to impart variable illumination to a thick photoresist (PR).[10,11] After a single exposure and developing step, the thickness of the developed photoresist is related to the exposure dose the PR received in each location, which allows for the creation of 3D surface features. The PR pattern is then transferred to the substrate material through an anisotropic etch process. The process is shown schematically in Figure 1. Grayscale processing has the advantage of being able to create arbitrary surface profiles, such as aspherical and off-axis arrayed lenses, that are not possible with other techniques such as polymer reflow.[12] Moreover, these lenses can be arrayed with 100% fill factor and are not limited by diffusion processes. However, while conceptually a simple process, much effort must be put into properly determining the non-linear relationship between exposure dose and resulting developed photoresist thickness. This nonlinearity can be reduced but not completely eliminated by a combination of optimizing exposure, developing, and etching processes. As a result, the design process for creating grayscale features is iterative, with extremely good characterization of the resulting photoresist thickness as a function of: exposure dose, development conditions, and etching processes necessary to replicate the desired features well.

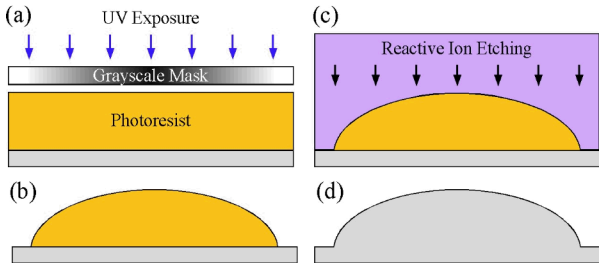

Figure 1. Grayscale processing (a) exposure of a photoresist with an optically graded grayscale mask (b) 3D photoresist profile after exposure and development, (c) transfer of the pattern to the substrate with reactive ion etching, and (d) resulting surface relief etched into substrate.

2. DESIGN

This optic is designed to fully integrate with a microfabricated linear surface-electrode ion trap.[2,9] A schematic of the operation of the lens is shown in Figure 2. The purpose of the excitation lens is to take the 397 nm output of a single mode fiber that is 732 μm from the backside of the lens substrate and deliver it to the trapped Ca^+ ion near the surface ion trap. The input light passes through a lithographically defined gold aperture on the backside of the fused silica substrate on its way to the grayscale refractive lens on the front side of the substrate. This backside aperture causes the lens to be slightly underfilled so that only the middle 64 μm diameter of the lens will be filled. This underfilling relaxes the targeted illuminating tolerances with respect to ion trapping location. The lens focuses the 397 nm excitation wavelength onto an ion that is held 149 μm from the plane of the lens. The grayscale lenses were designed to have comparable performance to an equivalently configured diffractive optical element (DOE) with respect to wafer thickness, imaging distances, and aperture. The same optical configuration layout was implemented in a fluorescence collection function (also utilizing an arrayed DOE).[9]

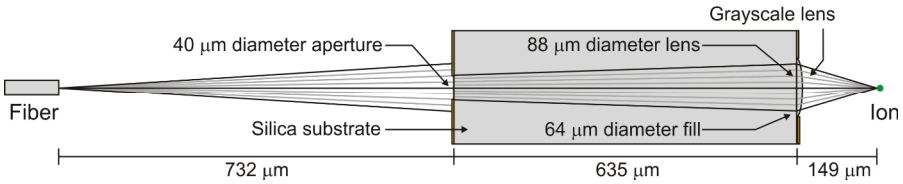

Figure 2. Schematic of the lens in operation. The 397 nm light exits the singlemode fiber on the left and is focused on the ion. The surface of the ion trap is on the right.

The grayscale lens was designed as an aspherical (conic) microlens with zero on-axis spherical aberration described by

$$z = \frac{cr^2}{1+\sqrt{1-c^2r^2(\kappa+1)}} \quad (1)$$

where r is the radial coordinate, κ is the conic constant, and c is given by $1/R$ where R is the radius of curvature. A cross section and associated grayscale fracture level of the ideal lens profile are shown in Figure 3(a) and Figure 3(b). Lens design details are given in Table 1.

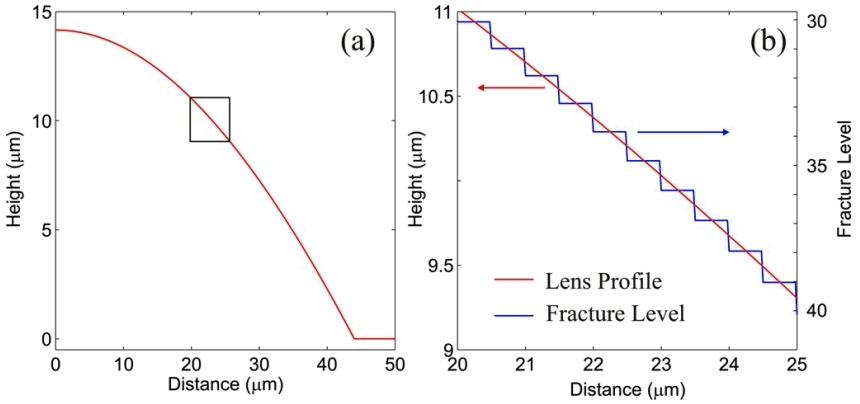

Figure 3. (a) ideal lens profile and (b) lens profile with fracture level zooming in on the area indicated in the small box in (a).

Table 3. Lens definition

Sag	14.16 μm
Lens Diameter	88 μm
Radius of curvature	62.30 μm
Conic Constant	-1.851
Wafer Thickness	635 μm

3. FABRICATION

Once the design was finalized, the calibration of the photoresist (PR) thickness to mask optical density (OD) was begun. We used an I85-B high energy beam sensitive (HEBS) glass calibration plate from Canyon Materials. The main portion of this mask is dedicated to a series of 200 uniform gray levels that correspond to an OD from 0.152 and 2.0. On exposure, the developed pattern will have 3 200 x 800 μm rectangles of each grayscale level 1 through 200. Profilometry measurements of these features then calibrate the photoresist exposure time, develop conditions, and final photoresist thicknesses to optical density. The exposure and development process was optimized to allow for the greatest access to grayscale levels/optical densities.

Simultaneous to this work, an etching process was developed to transfer the thick patterns to the underlying substrate through an inductively coupled plasma reactive-ion etching (ICP-RIE) tool. Thick cylindrical pillboxes and reflowed lenses with approximate packing density to the final part were transferred into the fused silica substrate. These conditions were finely tuned to achieve selectivity of etching rate of PR to silica of close to 1. Because our ultimate etch selectivity was so close to one, we did not have to significantly modify the exposure and develop step to achieve proper lens profiles.

The final layout in the grayscale lens began once the relationship between mask optical density and resulting PR thicknesses were experimentally determined. The optimal lens profile, as determined by Equation (1), is discretized into a finite number of of steps using constant horizontal step widths as illustrated in Figure 3(b). The height of each step is determined by the height in the middle of the horizontal zone. A lens of diameter, D, is broken up into N zones where the height of the nth zone is given by

$$h(n) = \frac{D}{2}\left(\frac{n-1/2}{N}\right) \; for \; (n = 1,2,3 \ldots N) \; . \tag{2}$$

An example of fracturing to a constant zone width of 0.5 μm is shown in Figure 3(b). Scripts were written to discretize the lens layouts into individual pixels 0.5 μm on a side in the DW-2000 mask creation tool. The mask optical density was designed to range from 0.152 to 1.845 in 88 steps. The mask data was exported to the common GDSII file format for fabrication by both Canyon Materials and the University of Delaware.

Substrates of 3 inch diameter, 635 μm thick fused silica procured from Valley Design were coated with the PR and exposed and developed according to the described process to give 3D profiles of the lenses. The patterns were then transferred to the substrate via the ICP-RIE process. The optimal etching conditions in the inductively coupled plasma reactive-ion etcher was using a chemistry of CHF_3, CF_4, and Ar in ratios of 3:4:4 for a total time of 90 min for the 14.2 μm sag. A critical issue for the etching was adequate thermal control of the wafers. Localized heating caused non-uniformity and run away etching. An example of a badly etched lens is shown in Figure 4(b). Improper etching was avoided with proper wafer submounting using Crystal Bond to the silicon carrier wafer.

To complete the device, a top metal layer was deposited on the surface to define device packages and the 88 μm lens apertures as shown in Figure 4(a). This layer was a film of 1 μm thick gold to prevent light transmission. Backside apertures of 40 μm were deposited on the fused silica substrate to align with the individual lenses on the front side of the device. An individual lens realized in silica is shown in Figure 4(c).

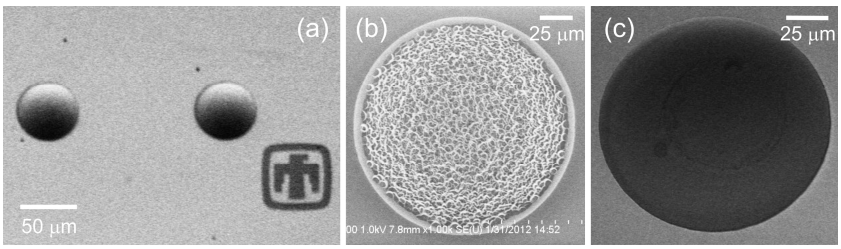

Figure 4. SEMs of the (a) an array of lenses (b) an individual lens after a bad etch, and (c) a lens after a successful etch.

4. CHARACTERIZATION AND TESTING

The finished lenses were characterized by stylus profilometry and a WYKO NT9800 white-light optical profiler. A sample cross section obtained by light profilometry is shown in Figure 5. Due to the large sag (>14 μm) there was data dropout at depths between ~10 and 14 μm due to the collection aperture of the profilometer optics. The lens overall has a smooth profile and agrees well with a least-squares-fit to the optimal designed profile. As seen in Figure 5, the fabricated lens has a shorter sag than the design, with a height of 13.7 μm compared to the 14.2 μm of the design.

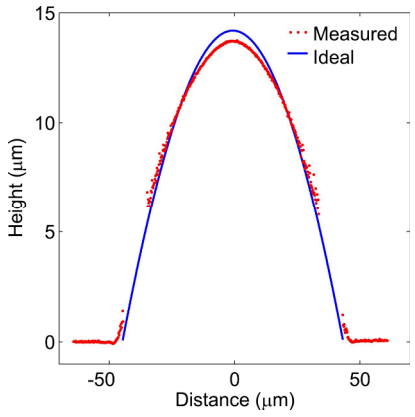

Figure 5. Cross section of a lens obtained from white light interferometry with the fit of an ideal cross section overlaid.

Initially it was thought that discolored regions evident in the SEM pictures - faintly visible in Figure 4(c) - were regions of roughness. However both stylus and white light profilometry indicated the lenses were fairly smooth. The root mean square (RMS) roughness calculated from the middle 25 μm square region at the top of the lens of the white light profilometry data gave a surface roughness of ~36 nm. Detailed radial variation of the surface roughness was obtained by noncontact AFM (Digital Instruments Dimension 3100) using an NSC15 tip fabricated by Mikromask. A representative AFM image near the edge of the lens l is shown in Figure 6(a). Small 5 x 5 μm sections of the lens were examined as a function of radial distance from the middle. These images were flattened to a second order before the RMS values were calculated. The RMS roughness as a function of radial distance is shown in Figure 6(b). Note that the lens surface becomes rougher moving away from the center of the lens, which corresponds to the material near the edges of the lens being exposed to the etch for longer times. Even thought this data is not as reliable due to tip convolution effects and measures much lower than the interferometry data, is shows that the roughness of the lens increases in a radial direction as expected since the edges of the lenses were exposed to etch conditions for a longer time

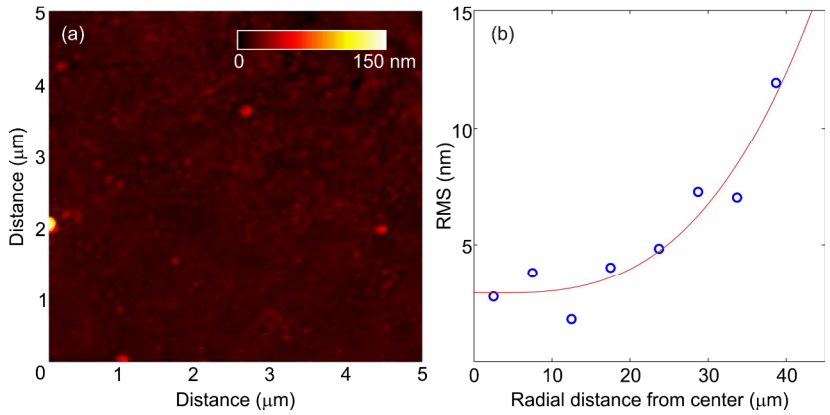

Figure 6. (a) a representative AFM image of the lens surface with an inset height scale bar and (b) roughness as a function of radial distance from the middle of the lens.

The beam waist and focal length of the lens was determined by scanning knife edge experiments as shown in Figure 7.[13] A Mikron laser tuned to 397 nm at 120 mW power is used as the source which was split and 50% of signal sent to reference photodetector. The other beam is coupled into Nufern single mode fiber with an NA of 0.12. Both beams are modulated with a chopper at 300 Hz to improve signal to noise. The lens assembly was held in place on a XY translation/rotation stage. The fiber output was aligned to the back aperture of the lens assembly with a XYZ translation/tip/tilt chuck. A silicon v-grove edge serves as the razor edge that is translated by computer control perpendicular to the optical axis. A Si photodiode is used to capture the transmitted signal. Transmitted and reference signals were collected simultaneously by computer. The beam diameter was determined by finding the $1/e^2$ values of the collected intensity.

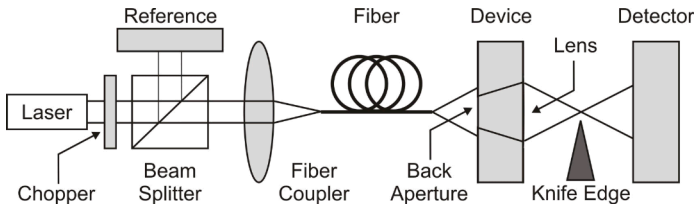

Figure 7. Knife edge test setup

5. RESULTS AND DISCUSSION

Knife edge measurements of the spot size moving through the focus of three different lenses on the same wafer found the focal size to be 2.6 μm diameter at a focal length of 149 μm which was the desired focal length. A plot of the through-focus beam waist of a lens is shown in Figure 8. The lens efficiency was calculated by measuring the total incident power passing through a backside aperture and through the front surface of the glass (no lens or front side aperture) taking into account Fresnel losses. The power found in the beam waist at the focus of the lens was then divided by the total input power from the bare aperture to yield the efficiency. The measured efficiencies for the 3 lenses were 0.67, 0.76, and 0.79. The maximum measured efficiency of the grayscale lens was 79%, which is 86% of the theoretical maximum of 92% considering Fresnel losses.

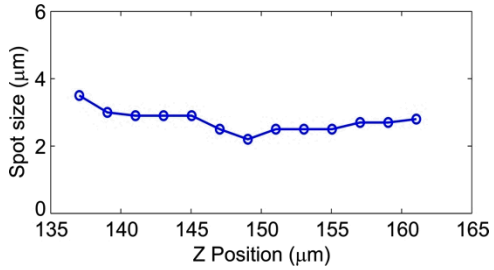

Figure 8. Zscan data from a grayscale lens

These efficiency values are slightly complicated by the fact the entire front side of the glass was also etched uniformly during the pattern transfer step. This means that the top surface of the glass on the same side as the lenses had a roughness on the order of ~60 nm. Since the clear aperture used to measure total power were defined on this surface, the open aperture measurement also contained scattering losses from the roughened surface. This would complicate the measurement of the input power since scattering losses may send power away from the detector. Since the bare apertures are the roughest regions of the wafer, the scattering losses could be higher in the bare apertures than in the smoother lenses.

We can use the roughness values to estimate the transmitted rays affected by scattering and that effect on efficiency. The total diffuse transmittance resulting from surface scatter is given by

$$T^S = T_O\left\{1 - exp\left[-\left(\frac{2\pi\Delta n\sigma}{\lambda}\right)^2\right]\right\} \tag{3}$$

where σ is the surface RMS roughness, Δn is the difference between the two media (0.47), and λ is the wavelength of light (397 nm).[14,15] The calculated diffuse scatter for the middle portion of the lenses using the interferometry measured RMS of 37 nm corresponds to a diffuse scatter decrease of 7.3%. The open aperture, with an RMS roughness of ~60 nm, corresponds to a decrease of ~20%. Since the forward scatter from a surface is most likely Lambertian, it could be that the effect of the diffuse scattering losses for the lenses has greater impact than the same effect from the open aperture. The measurement of total power into the lens from the open aperture is collected using the entire field of the detector; therefore, more of the diffusely scattered light could be collected. In the lens, the power measured at the focus is less likely to contain diffusely scattered light. It is not clear, so far, which surface's scattering effect dominates the efficiency measurements.

The roughness of the lens surface is an important aspect of fabrication of low noise and low scatter optical components for use in quantum applications. Optical finish on lenses is desired to be < λ/100. The required use of 397 nm light makes scatter from these optical surfaces worse, as scattering losses increase as the wavelength gets shorter. To make low-scatter micro-optics smoother surfaces must be created. Subsequent refinement of the etch step yielded very smooth lens profiles with RMS roughness < 5 nm and open apertures with roughness < 3 nm, but these refined etch parameters have not been used to create fully apertured and integrated lenses. The scattering losses from such smooth surfaces at 397 nm are <0.005%, which would dramatically reduce the scattered light in the system.

Finally, simulations of the full test setup as shown in Figure 2, using the actual numerical aperture of the Nufern illumination fiber were performed with Zemax. A simple conic fit to the lens surface from the middle 60 μm diameter of the interferometry data yielded a ROC = 69.8 μm and a conic constant of -3.082, which is shown in Figure 9 overlaid on the actual lens profile. This prescription and simulated illumination conditions gave the focal plane at 183 μm, which

was longer than the 149 μm we measured. The spot size was diffraction limited over a propagation range of z = 6 μm with a beam waist of < 3 μm.

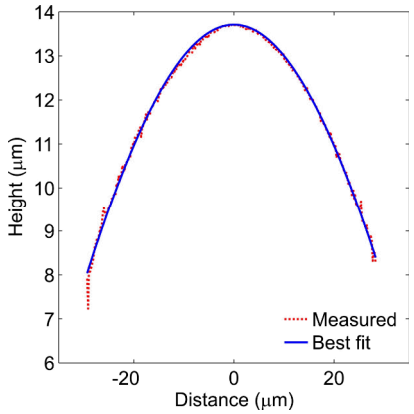

Figure 9. A cross section of the middle 60 μm of the lens obtained from white light interferometry with the best fit overlaid.

6. CONCLUSIONS

We have designed and fabricated a grayscale aspheric micro-lens in fused silica to be integrated with ion trapping fixtures. The lens was first formed in thick photoresist using grayscale lithography, and then transferred to the silica substrate through reactive ion etching. The fabricated lens matched the lens profile well, and the measured focal length and spot size of 149 μm and 2.6 μm agreed exactly with the intended design. The maximum measured efficiency was ~80%, which compares favorably with the theoretical limit of 92% due to Fresnel losses. Surface roughness of the lenses must be lowered to reduce diffuse scatter from the lens surface, especially for the demanding noise requirements of quantum manipulation of trapped ions. Further refinement of the process to exactly reproduce the desired lens profile is also necessary. Despite these limitations, the grayscale refractive micro-optic demonstrates a clear path forward for the creation of low loss, low scatter optics necessary in the creation of addressable trapped ion arrays.

Acknowledgements

This work was supported by IARPA. Sandia National Laboratories is a multi-program laboratory managed and operated by Sandia Corporation, a wholly owned subsidiary of Lockheed Martin Corporation, for the U.S. Department of Energy's National Nuclear Security Administration under contract DE-AC04-94AL85000.

REFERENCES

[1] D. J. Wineland and D. Leibfried, "Quantum information processing and metrology with trapped ions," Laser Physics Letters 8(3), 175-188 (2011).
[2] D. T. C. Allcock, T. P. Harty, H. A. Janacek, N. M. Linke, C. J. Ballance, A. M. Steane, D. M. Lucas, R. L. Jarecki, S. D. Habermehl, M. G. Blain, D. Stick and D. L. Moehring, "Heating rate and electrode charging measurements in a scalable, microfabricated, surface-electrode ion trap," Applied Physics B 107(4), 913-919 (2011).
[3] D. L. Moehring, C. Highstrete, D. Stick, K. M. Fortier, R. Haltli, C. Tigges and M. G. Blain, "Design, fabrication and experimental demonstration of junction surface ion traps," New Journal of Physics 13(7), 075018 (2011).
[4] A. Myerson, D. Szwer, S. Webster, D. Allcock, M. Curtis, G. Imreh, J. Sherman, D. Stacey, A. Steane and D. Lucas, "High-Fidelity Readout of Trapped-Ion Qubits," Phys. Rev. Lett. 100(20), (2008).
[5] D. P. DiVincenzo, "The physical implementation of quantum computation," Fortschritte Der Physik-Progress of Physics 48(9-11), 771-783 (2000).
[6] A. VanDevender, Y. Colombe, J. Amini, D. Leibfried and D. Wineland, "Efficient Fiber Optic Detection of Trapped Ion Fluorescence," Phys. Rev. Lett. 105(2), (2010).
[7] D. J. Wineland, J. C. Bergquist, W. M. Itano and R. E. Drullinger, "Double-resonance and optical-pumping experiments on electromagnetically confined, laser-cooled ions," Optics Letters 5(6), 245-247 (1980).

[8] D. T. C. Allcock, J. A. Sherman, D. N. Stacey, A. H. Burrell, M. J. Curtis, G. Imreh, N. M. Linke, D. J. Szwer, S. C. Webster, A. M. Steane and D. M. Lucas, "Implementation of a symmetric surface-electrode ion trap with field compensation using a modulated Raman effect," New Journal of Physics 12(5), 053026 (2010).
[9] G. R. Brady, A. R. Ellis, D. L. Moehring, D. Stick, C. Highstrete, K. M. Fortier, M. G. Blain, R. A. Haltli, A. A. Cruz-Cabrera, R. D. Briggs, J. R. Wendt, T. R. Carter, S. Samora and S. A. Kemme, "Integration of fluorescence collection optics with a microfabricated surface electrode ion trap," Applied Physics B 103(4), 801-808 (2011).
[10] W. Daschner, P. Long, R. Stein, C. Wu and S. H. Lee, "General aspheric refractive micro-optics fabricated by optical lithography using a high energy beam sensitive glass gray-level mask," Journal of Vacuum Science & Technology B 14(6), 3730-3733 (1996).
[11] T. Dillon, M. Zablocki, J. Murakowski and D. Prather, "Processing and modeling optimization for grayscale lithography," in *Proceedings of the SPIE*, p. 69233B (2008).
[12] D. Daly, R. F. Stevens, M. C. Hutley and N. Davies, "The manufacture of microlenses by melting photoresist," Measurement Science & Technology 1(8), 759-766 (1990).
[13] Y. Suzaki and A. Tachibana, "Measurement of μm sized radius of gaussian laser-beam using scanning knife-edge," Appl Optics 14(12), 2809-2810 (1975).
[14] A. Poruba, A. Fejfar, Z. Remes, J. Springer, M. Vanecek, J. Kocka, J. Meier, P. Torres and A. Shah, "Optical absorption and light scattering in microcrystalline silicon thin films and solar cells," J. Appl. Phys. 88(1), 148-160 (2000).
[15] J. Krc, F. Smole and M. Topic, "Analysis of light scattering in amorphous Si : H solar cells by a one-dimensional semi-coherent optical model," Progress in Photovoltaics 11(1), 15-26 (2003).